ChemComm

Chemical Communications

www.rsc.org/chemcomm

Number 12 | 28 March 2008 | Pages 1365–1480

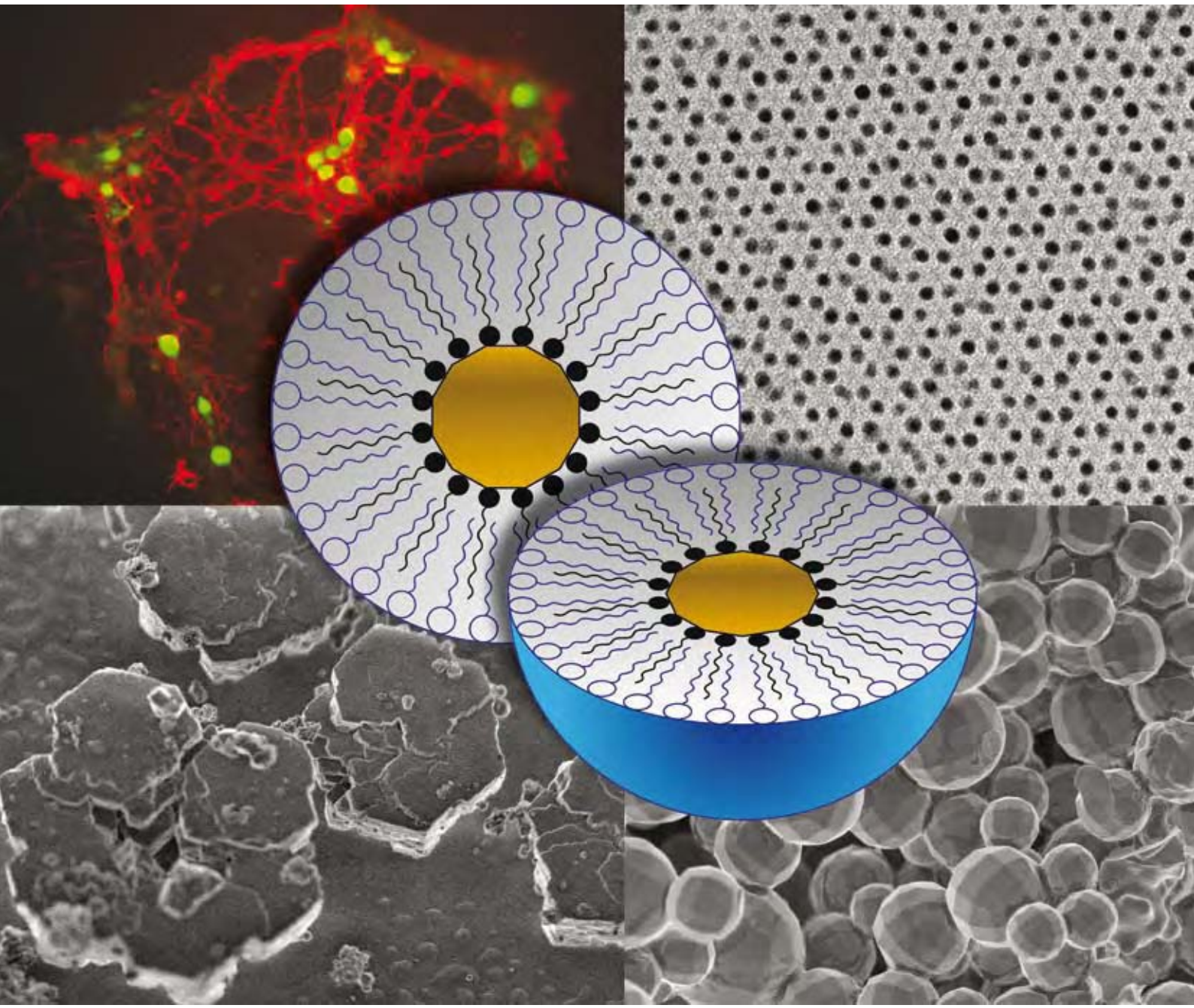

ISSN 1359-7345

RSC Publishing

1359-7345(2008)12;1-7

Nanocrystal-micelle: synthesis, self-assembly and application

Hongyou Fan*[ab]

Received (in Cambridge, UK) 23rd July 2007, Accepted 15th November 2007
First published as an Advance Article on the web 6th December 2007
DOI: 10.1039/b711251n

Nanocrystals (NCs) are one of the important building blocks for fabrication of nanostructured arrays for wide range of optical, electronic, magnetic, catalytic and biosensing applications. Here, our recent advances in the synthesis, self-assembly and application of NC-micelles are highlighted. The NCs are encapsulated inside the core of surfactant micelles in a rapid, interfacially driven micro-emulsion process. The flexible surface chemistry of the NC-micelles causes them to be water-soluble and allows further self-assembly into two- and three-dimensional ordered arrays. The NC-micelles are biocompatible, of interest for bio-labeling. Finally, integration of the ordered arrays and charge transport property are discussed.

Introduction

Nanocrystals (NCs) exhibit unique size- and shape-dependent physicochemical properties arising from low-dimensional quantum confinement effects and have a wide range of potential applications in areas such as optics, electronics, catalysis, magnetic storage and biological sensing.[1–5] NCs have been successfully used as building blocks for the fabrications of 2- and 3-D NC arrays for the development of 'artificial solids' (or metamaterials) with new collective optical and electronic properties derived from the interaction or coupling of nearest neighbour NCs in an assembly, leading to a wide range of potential applications in areas such as optics, electronics, magnetic storage and sensor platforms.[2,6–12] For example, In 2-D quantum dot monolayers formed in a Langmuir trough, Collier *et al.*[8] reported quantum mechanical tunneling between adjacent silver NCs at an interparticle spacing below 1.2 nm and a reversible insulator-to-metal transition below 0.5 nm. Even richer transport and collective phenomena are expected for 3-D NC arrays.[13] Zeng *et al.*[12] observed magnetic coupling within magnetic NC arrays. Using uniformly-sized CdSe NCs passivated with a close-packed monolayer of organic coordinating ligands (trioctylphosphine oxide), Murray *et al.*[14] exploited the inherent tendency for monodisperse lyophobic colloids to self-assemble to create periodic, three-dimensional quantum dot superlattices. Following this approach, Klimov *et al.*[10,15] prepared ordered CdSe quantum dot films and demonstrated optical gain and stimulated emission.

Microscopically, formation of ordered NC arrays relies on balancing nanoparticle attractions and interaction through forces such as charge interaction, van der Waals interactions, hydrogen bonding, *etc*. On this aspect, NC surface chemistry is crucial for controlling the nanostructure in final ordered NC arrays. For example, carboxylic acid groups have been functionalized on the NC surfaces to induce hydrogen bonding between NCs and form quasi-honeycomb hexagonal close packing and simple cubic packing.[16] Through tuning NC surface charges and charge numbers, diamond-like non-close packed NC arrays were observed through TEM imaging.[17] Linear NC arrays through cross-linking difunctionalized NCs using a molecular linker.[18] Macroscopically, the ordered NC arrays have been formed through varied processes. The most studied process involves evaporation of a drop of NC organic solution on solid substrates (TEM grid, mica or HOGH, *etc*), forming face-centered-cubic (fcc), body-centered-cubic (bcc) or hexagonal-close-pack (hcp) superlattice films.[3,19,20] Collier

[a] *Sandia National Laboratories, Advanced Materials Lab, 1001 University Blvd. SE, Albuquerque, New Mexico 87106, USA. E-mail: hfan@sandia.gov; Fax: +01 505-272-7336; Tel: +01 505-272-7128*
[b] *The University of New Mexico/NSF Center for Micro-Engineered Materials, Department of Chemical and Nuclear Engineering, Albuquerque, New Mexico 87131, USA*

Hongyou Fan

Hongyou Fan earned a BS degree in the Department of Chemistry at Jilin University in 1990, a MS degree in 1995 from Changchun Institute of Applied Chemistry in the field of polymer chemistry and physics, and a PhD degree in 2000 from the University of New Mexico in the field of nanoporous materials and composites. Currently He is a Principal Member of the Technical Staff at Sandia National Laboratories, Albuquerque, New Mexico. He also holds an adjunct professor position in the Department of Chemical and Nuclear Engineering at the University of New Mexico. His research focuses on the development of new synthesis methods and self-assembly processes to fabricate multifunctional nanomaterials, fundamentally understanding self-assembly mechanism, structural evolution from molecular level to nano- and microscale, and understanding structure–property relationships. He received an R&D 100 Award in 2007 for the development of a simple, economical nanotechnology coating process for nanoparticle optical, electrical and magnetic thin films. For more information, please visit his group webpage: http://www.unm.edu/~hyfan.

et al.[8] reported a Langmuir–Blodgett process to form a 2-D hexagonal close-packed superlattice film of silver NCs. A heterogeneous precipitation process and formation of superlattice solids were reported and carried out by slow addition of nonsolvents into a NC organic solution.[21] Over long time aging, well-shaped crystal superlattice solids with fcc structure were finally obtained.

Previous extensive efforts in fabrication of NC arrays have been focused on using alkane-chain capped monodisperse NCs.[4,13,22] These NCs are hydrophobic and chemically inert. Consequently, ordered NC arrays were formed by balancing the forces of interparticle attraction and van der Waals interaction due to alkane chain interdigitation. The alkane chain interdigitation has been demonstrated to be thermodynamically favorable for the stability of the final NC arrays.[23] Yang and co-workers[24] demonstrated the patterned magnetic NC arrays combining the soft lithography method. Recently, NC self-assembly has been extended to form arrays with two compositions and varied crystal structures.[25–27] Progress has been recently made in the synthesis of hierarchically ordered NC/polymer macrostructures by combined self-assembly of metal or semiconductor NCs with polymers through the ''Breath figure'' method.[28–30]

The common problem associated with the above approaches is that alkane chain capped NCs are hydrophobic and soluble only in organic solvents. The van der Waals interactions between interdigitated alkane chains surrounding the NCs result in weak mechanical and thermal stability which is not ideal for the fabrication of reliable devices. It is desirable to incorporate NCs in inorganic thin film matrices such as silica or titania for achieving chemical, thermal and mechanical robustness and enhanced device functionality.[31–34] Earlier efforts have focused on encapsulation of metal NCs inside sol–gel matrices.[35–37] Recently, mesoporous materials have been used as templates to create composite materials with metal or semiconducting NCs.[38–42] There are several disadvantages associated with the above methods: first, the NC arrays inside the host materials exhibit poorly defined or less ordered structures. This is problematic to get reproducible results in structure and device measurements. Second, the methods have less control over particle sizes and loading. Finally, it is difficult to precisely control interparticle spacing that is essential for achieving collective physical properties.[8,12,43,44] These combined factors ultimately limit routine integration of NCs into 2- and 3-D artificial solid devices, in which electronic, magnetic and optical properties could be tuned through electron charging and quantum confinement of individual NCs mediated by coupling interactions among neighboring NCs.[8,12,44]

In this article, our recent advances on the synthesis of a new building block – *NC-micelle*,[9,45,46] its self-assembly[45,47–49] and applications in optical[34] and electric[9,34] integration and bioimaging[50] are summarized. Using the NC-micelle as a building block, we demonstrated the formation of highly ordered NC arrays in inorganic frameworks through several self-assembly processes such as hydrothermal process, evaporation process, *etc*. These ordered arrays provide a model system for study of collective behavior of the NC assembly.

2 Synthesis of NC-micelles

The key to stabilizing hydrophobic NCs in an aqueous phase is to reduce NC/water surface tension. We envisioned organically-passivated NCs as large hydrophobic molecules that, if incorporated individually into the hydrophobic cores of surfactant micelles, would result in the formation of NC-micelles composed of a metallic NC core and a hybrid bilayer shell with precisely defined primary and secondary layer thicknesses (see Fig. 1).[9] The hydrophilic NC-micelle surface would cause them to be water-soluble and allow further assembly or functionalization as depicted in Fig. 1.

To synthesize NC-micelles, a micro-emulsion procedure was developed first (see Fig. 2). A concentrated NC solution, prepared in organic solvents (chloroform, hexane, *etc*.), was

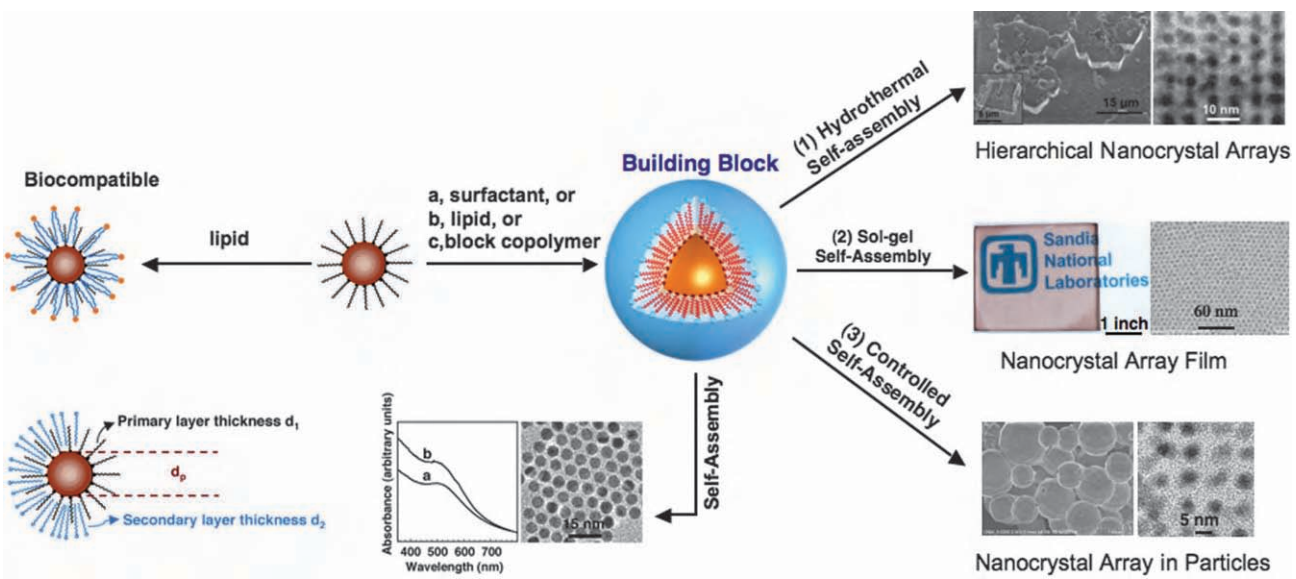

Fig. 1 Schematic illustration of the synthesis of water-soluble and biocompatible gold NC-micelles and formation of periodically ordered gold NC/silica arrays through varied self-assembly processes.

added to an aqueous solution of surfactants under vigorous stirring to create an oil-in-water micro-emulsion. Organic solvent evaporation transferred the NCs into the aqueous phase by an interfacial process driven by the hydrophobic van der Waals interactions between the primary alkane of the stabilizing ligand and the secondary alkane of the surfactant, resulting in thermodynamically defined interdigitated bilayer structure (Fig. 1). The interdigitated bilayer is the driving force for the stability of the NC-micelle structure. This was evidenced by the three endothermal peaks appearing at $\sim$11.5 °C for the NC-C12TAB sample, $\sim$47 °C for the NC-C14TAB sample, and $\sim$72 °C for the NC-C16TAB sample from differential scanning calorimetry (DSC) experiments on the dried powder samples of gold NC-micelles that were prepared using DT-stabilized gold NC and surfactants with different alkane chain lengths (C12TAB, C14TAB and C16TAB).[45] The temperature of the peak maxima increased with increasing alkane chain length. This suggested that longer alkane chains contributed to more extensive van der Waals interactions.[51,52] For single-tailed surfactants, an alkane chain of eight or more carbons was required to stabilize NC-micelles, with gold NCs stabilized by C_{12} alkanethiols (dodecanethiol).

The surfactant encapsulation was accomplished in a single, rapid (10 min) step of solvent evaporation. In our method, the stabilization of hydrophobic NCs in the aqueous phase relies on the thermodynamically favorable interdigitation of surfactants and NC stabilizing ligands formed after solvent evaporation, enabling rapid efficient transfer of the NCs into the aqueous phase. The method provides several advantages: (1) the encapsulation process involves no chemical reactions, and therefore would not change the physical properties (optical, electronic, *etc*) of the original NCs.[50,53] (2) The encapsulation process is simple and flexible through the use of varied surfactants and block copolymers, such as cationic, anionic and non-ionic surfactants, to form NC-micelles, allowing facile control of micelle surface charge and functionality; (3) the densely packed interdigitated surfactant bilayers behave like a barrier layer that may help to prevent NC-micelle aggregation or core NC oxidation, thus preserving their physical properties. Finally, phospholipids can be used to form biocompatible NC-micelles for bioimaging and biosensing applications. A variety of commercial lipids with functional groups, such as –(OCH_2CH_2)OH, –NH_2, –COOH, –biotin, *etc*, can be used to enhance biocompatibility or for further bioconjugation.[50,54]

NC-micelle solutions usually remained the same color of the original hydrophobic nanoparticles and are very stable for several years. The numbers of NCs can be controlled through either NC concentration or surfactant concentration. For spherical gold NC-micelles, their monodispersity was confirmed by UV/visible spectroscopy (Fig. 1), where no difference was observed in the position or width of the plasmon resonance band ($\sim$510 nm) of the C_{12}-alkanethiol stabilized gold NCs in chloroform and the resulting water soluble NC-micelles.

In addition to spherical NCs, we have successfully extended the surfactant encapsulation technique to stabilize and self-assemble NCs with other shapes such as rods and cubes.[45] Transmission electron micrograph (TEM) images revealed that surfactant ''bilayer'' stabilized CdTe nanorods formed uniform arrays (Fig. 3(d)) while Fe_2MnO_4 NC-micelles self-organized into ordered arrays with cubic symmetry (Fig. 3(e)).

Depending on the surfactants, the final NC-micelle surface can be tuned through various functional groups. Through electrostatic interactions and/or hydrogen bonding, 2- and 3-D NCs arrays can be formed. Fig. 3(b) and (c) show some representative TEM images of 3-D gold NC superlattices.

In addition to our methods, several other methods to synthesize metallic, semiconducting and magnetic NC-micelles or similar structures have also been reported. For metal NCs, Patil *et al*.[51] reported the formation of an interdigitated bilayer that stabilized silver nanoparticles in the aqueous phase. Shen

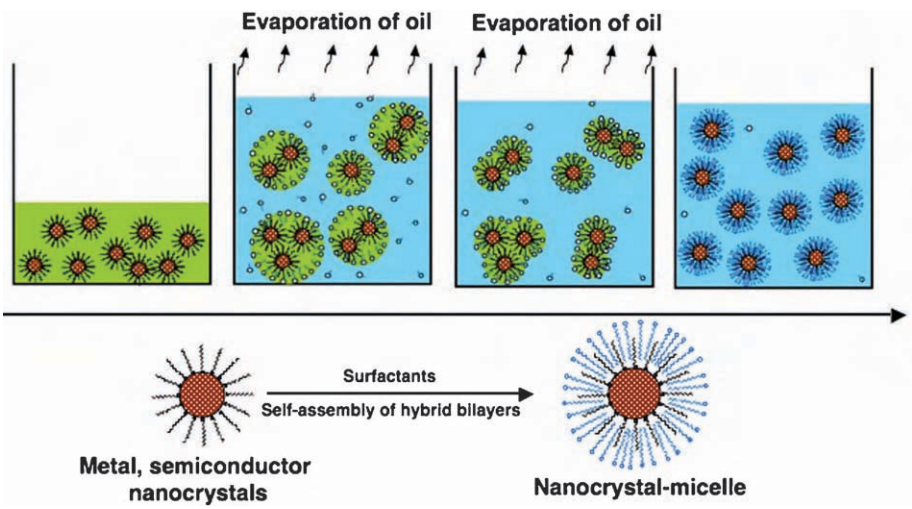

Fig. 2 Process scheme for the synthesis of water-soluble NC-micelles. Addition of an oil containing gold NCs into a surfactant containing aqueous solution during vigorous stirring leads to the formation of an oil in H_2O microemulsion. Subsequent evaporation of oil transfers the NCs into the aqueous phase by an interfacial process driven by the hydrophobic van der Waals interactions between the primary alkane of the stabilizing ligand and the secondary alkane of the surfactants, resulting in thermodynamically defined interdigitated bilayer structures surrounding individual NCs to make them water soluble. Adapted from ref. 9.

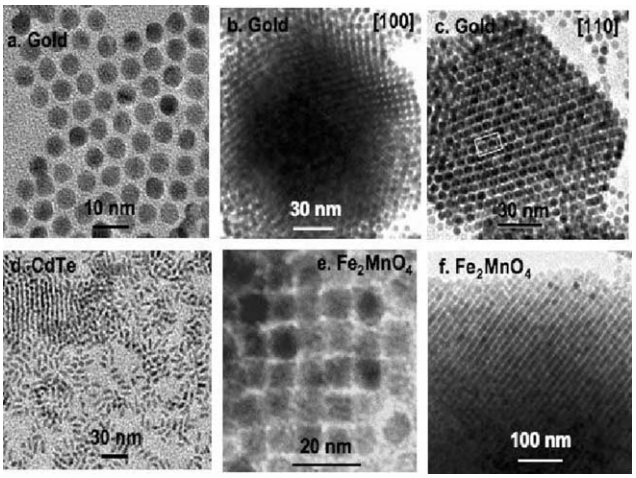

Fig. 3 TEM images of ordered NC-micelle arrays. (a) 2-D gold NC-micelle hexagonal arrays. (b) [100] orientation of 3-D gold NC-micelle arrays. (c) [110] orientation of 3-D gold NC-micelle arrays. (d) Ordered CdTe nanorod-micelle arrays. (e) 2-D Fe_2MnO_4 nanocube-micelle arrays. (f) [100] orientation of 3-D ordered Fe_2MnO_4 nanocube-micelle arrays. Adapted from ref. 45.

et al.[55] used a similar method to synthesize magnetic fluids. Euliss *et al.*[56] transferred hydrophobic maghemite nanoparticles into an aqueous medium using block copolypeptides. When the aqueous maghemite was combined with the block copolypeptide, the nanoparticles assembled into uniform clusters comprised of approximately 20 nanoparticles, resulting in a water-soluble block copolypeptide–nanoparticle composite structure. Ai *et al.*[57] synthesized magnetite-loaded polymer micelles and used them as ultrasensitive magnetic-resonance probes. Kim *et al.*[58] synthesized magnetic micelles using cross-linked amphiphilic block copolymers. Lecommandoux *et al.*[59] synthesized magnetic nanocomposite micelles and vesicles using amphiphilic poly(butadiene)-*b*-poly(glutamic acid) and magnetic iron oxide. Dubertret *et al.*[54] encapsulated individual NCs in phospholipid block-copolymer micelles and demonstrated both *in vitro* and *in vivo* imaging. When conjugated to DNA, the NC-micelles acted as *in vitro* fluorescent probes to hybridize to specific complementary sequences. Moreover, when injected into Xenopus embryos, the NC-micelles were stable, nontoxic ($<5 \times 10^9$ NCs per cell), cell autonomous, and slow to photobleach. Pellegrino *et al.*[53] reported a synthetic procedure for amphiphilic polymer coated NCs. Poly(maleic anhydride-*alt*-1-tetradecene) was used to decorate hydrophobic NCs with different materials. A cross linker, bis(6-aminohexyl)amine, was added to cross-link the polymer shell around each NC. Organosilane surfactant was used to encapsulate luminescent CdSe quantum dot clusters inside the micelles.[60]

3 Formation of biocompatible fluorescent NC-micelles and their use for neuron cell imaging

We have extended the surfactant encapsulation method to the synthesis of water-soluble, biocompatible semiconductor NC-micelles.[50] Monodisperse CdSe and CdSe/CdS core/shell NCs[61] were used to demonstrate the synthesis of fluorescent semiconductor NC-micelles. A concentrated suspension of NCs in chloroform was added to an aqueous solution containing a mixture of surfactants or phospholipids with different functional head groups such as ethylene glycol (–PEG) and amine ($-NH_2$). PEG was used to improve biocompatibility and amine groups provided sites for further bioconjugation. Addition of the NC chloroform suspension into the surfactant/lipid aqueous solution under vigorous stirring resulted in the formation of an oil-in-water microemulsion. Evaporation of chloroform during heating transferred the NCs into the aqueous phase by an interfacial microemulsion process, resulting in thermodynamically defined interdigitated bilayer structures. Based on evaluation of water-solubility and stability using UV-vis spectroscopy, TEM and fluorescent spectra, optimized lipids were those with at least 6–8 carbons in their hydrophobic alkane chains.

NC-micelle solutions exhibited the same visible and emission colors as hydrophobic NCs, as shown in the optical micrograph (Fig. 4(A)). As shown by UV-vis spectroscopy in Fig. 4(B), no difference was observed in the position or width of the absorbance bands at $\sim$480 and $\sim$590 nm from hydrophobic NCs and NC-micelles, which suggested that NC-micelles maintained their optical properties in water. Formation of ordered hexagonal close packing shown in TEM (Fig. 4(C)), as expected for individual monosized NCs, further confirmed the monodispersity of the NC-micelles. Photoluminescence (PL) spectra of NC-micelles exhibited no obvious shift in emission wavelength in comparison with those of the original NCs. Studies of photo-stability of these water-soluble NC-micelles under long-time laser irradiation showed that these NC-micelles exhibited no loss of PL intensity in water. The fluorescent lifetime of the CdSe/CdS-micelles was measured to be $\sim$30 ns. The stability of NC-micelles in a cellular aqueous environment was confirmed by incubation with rat hippocampal neurons (see below).

The biocompatibility of CdSe/CdS NC-micelles was evaluated in an initial study to examine their uptake in cultured rat hippocampal neurons. These biocompatible NC-micelles appeared to accumulate in intracellular vesicular compartments[62–64] in several cell types suggesting uptake may be mediated, at least in part, through endocytosis. Since synaptic vesicle recycling is tightly coupled to neurotransmitter release,[65] endocytosis could be manipulated by depolarization of the plasma membrane to excite neurons, evoking exocytosis for neurotransmitter release followed by endocytotic retrieval of synaptic vesicle membranes from nerve terminals. As shown in Fig. 5(A), NC-micelles (emission 592 nm, red) accumulated in neurons, distinguished by immmunohistochemical counterstain for NeuN (green), after exposure for 16 h in basal serum-free growth media. The retained fluorescence character after a fairly long incubation suggested the monodispersity and a general compatibility of the NC-micelles within a cellular environment.

To get a more deep view of NC uptake, We used pulse-chase labeling to expose hippocampal cultures to NC-micelles during membrane depolarization to trigger neurotransmitter release and coupled exo/endocytosis, followed by a return to basal media. NC fluorescence was monitored by confocal microscopy in widespread, yet clustered pattern surrounding

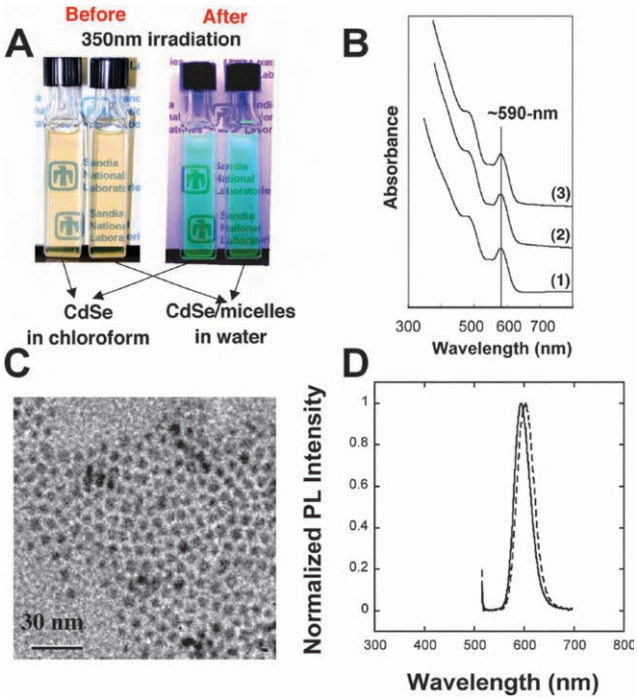

Fig. 4 (A) An optical micrograph of CdSe NCs in chloroform and CdSe-micelles in water prepared using CTAB. (B) UV-vis spectra of (1) CdSe/CdS in hexane, (2) CdSe/CdS-micelles prepared using 1,2-dioctanoyl-*sn*-glycero-3-phosphocholine (C8-lipid) and hexadecylamine (HDA), and (3) 1,2-distearoyl-*sn*-glycero-3-phosphoethanolamine-*N*-amino (polyethylene glycol) (aPEG) and dipalmitoyl phosphatidylcholine (DPPC). (C) TEM image of CdSe/CdS-micelles. (D) PL of CdSe/CdS in toluene (solid line) and C8-lipid encapsulated CdSe/CdS-micelles in water (dashed line). Adapted from ref. 50.

NeuN-positive neurons (Fig. 5(B)). This is consistent with a diffuse, punctate localization and uptake in neuronal processes and synapses. After exchange for basal media without NCs, there was an apparent time-dependent increase in the perinuclear accumulation of NC fluorescence accompanied by a decrease in the more widespread distribution seen immediately after KCl depolarization (Fig. 5(C) and (D)) after 5 h, NCs were effectively taken up by an endocytotic mechanism that was promoted by increased synaptic vesicle recycling and potentially followed by transport to lysosomes. This was evidenced by that the majority of NC fluorescence appeared to locate to a perinuclear compartment adjacent to NeuN stained neuronal nuclei. The results indicated a vesicular-mediated process for NCs fusing into lysosomal compartments.[66]

4 Synthesis of ordered NC arrays

NC-micelles afford flexible surface chemistry and function depending on the use of different surfactants. They retain the shape of the original hydrophobic NCs, which can be spherical, cubic and rod-like. Using the NC-micelle as a building block, we have demonstrated the formation of 2- and 3-D ordered NC arrays in several self-assembly processes including hydrothermal self-assembly process, evaporation-induced self-assembly process, and cooperative self-assembly process.

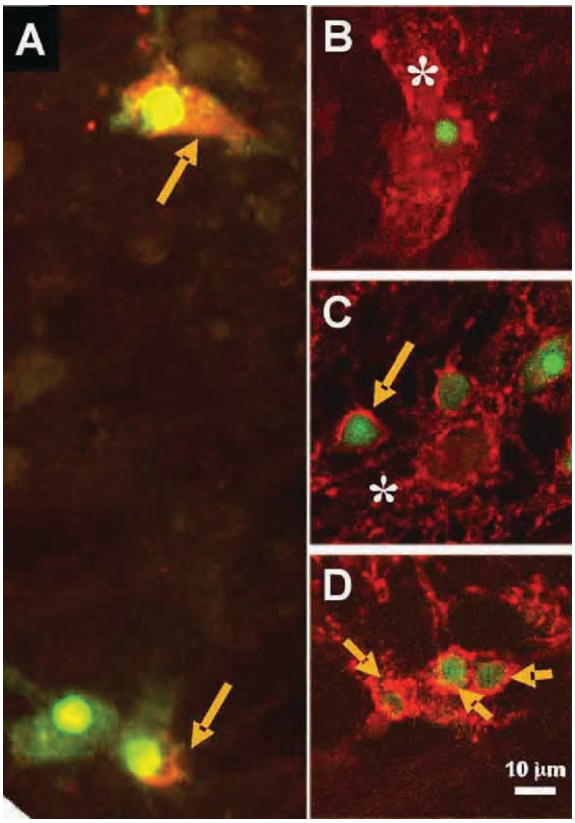

Fig. 5 Images of CdSe/CdS-micelles, prepared using aPEG, DPPC and HDA, in cultured rat hippocampal neurons. (A) Fluorescent microscopy image of NC accumulation (arrows) after 16 h of incubation ($\sim$1 mg ml^{-1} QD-micelles) in neurons identified by nuclear staining for NeuN (green). (B–D): Confocal microscopy of pulse-chase labeling with NC-micelles. Incubation with NC-micelles during depolarization with 55 mM KCl for 10 min (B) shows dispersed, punctate staining (indicated by asterisks) characteristic of neurite processes; whereas after chase in basal media without NP-micelles for 1 h (C) or 5 h (D) shows increasing perinuclear localization (arrows) with a corresponding decrease in the punctate stain seen in the 10 min labeling. Adapted from ref. 50.

4.1 Synthesis of hierarchically ordered mesostructured NC arrays

Through a hydrothermal self-assembly process, the NC-micelles were successfully utilized as building blocks in the synthesis of new, supported, and hierarchically ordered inorganic mesophase crystals.[48] Unlike the inert alkane chain capped NCs, NC-micelles provide multifunctional interface for further self-assembly with metal oxides through charge interactions and hydrogen bonding, which is analogous to the self-assembly of surfactant mesophases with metal oxides.[67] Depending on the substrates, these crystals consisted of either individual or subunit crystals. Inside these mesophase crystals, the gold NCs were assembled as an fcc mesostructure with oriented features.

The process (shown in Fig. 1) involved two steps: (1) preparation of a building block solution and (2) hydrothermal

nucleation and growth of mesophase crystals. In the first step, the NC-micelles were synthesized through a surfactant encapsulation process (Fig. 1, process (1)). The second step involved the nucleation and growth of mesophase crystals in a hydrothermal self-assembly process. Bis(triethoxylsilyl)ethane (BTEE) was used as the precursor.

Well-shaped and oriented NC/silsesquioxane crystals with face-centered cubic mesostructure began to grow over several hours and covered the whole substrate. Fig. 6(A) shows a typical SEM micrograph of large area arrays of the mesophase crystals grown on glass slides. These crystals were fairly uniform in shape and size ($\sim$15 μm) with flower-like hierarchical structure, which consists of three to five subunit crystals with hexagonal shape and size of $\sim$7 μm. A cross-sectional view of a crystal (Fig. 6(B), inset) shows that the mesophase crystal was about $\sim$8 μm high. TEM images (Fig. 6(C) and (D)) and low-angle XRD (see Fig. 7) reveal that the gold NCs self-assembled as an fcc mesophase inside these crystals. TEM images (Fig. 6(C) and (D)) show [110] and [100] orientations of the NC mesophase along with its corresponding selected electron diffraction pattern. The TEM images were consistent with a unit cell of $\sim$10.6 nm and a uniform, minimum interparticle spacing of $\sim$3 nm. The formation process involved a nucleation and growth self-assembly process, which was monitored using XRD (Fig. 7) and SEM (Fig. 8). Within the initial 10 min, the macroscopic crystals (size $<$0.5 μm, Fig. 8) begun to nucleate with no recognizable shape. At this stage, the NCs had started to self-assemble, exhibiting short range order. This was evidenced by the small hump between 2θ 2–3° in XRD patterns (Fig. 7(A), curve a). After 20 min, triangle-shaped crystals with size from 0.5 to 1 μm appeared. XRD patterns showed two peaks at low angle corresponding to cubic symmetry. Between 30 and 40 min, uniform hexagon-shaped subunit crystals with size of 7 μm were developed. Some of them merged into hierarchical structures. XRD (Fig. 7(A) curves (c) and (d)) showed that the fcc mesophase

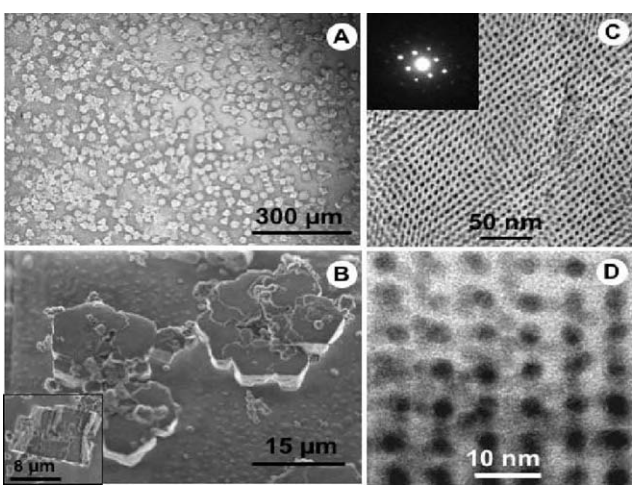

Fig. 6 SEM and TEM images of hierarchical NC mesostructure arrays on glass slides. (A) A low resolution SEM image. (B) A magnified SEM image of (A). Inset shows a cross-sectional image. Representative TEM images from (C) [110] orientation and (D) [100] orientation. The inset of (C) shows the selected area electron diffraction pattern from the image in (C). Adapted from ref. 48.

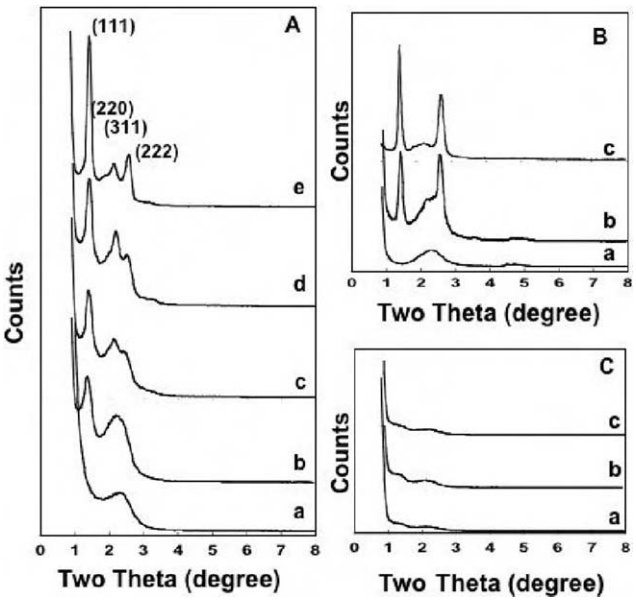

Fig. 7 (A) XRD patterns of hierarchical NC arrays on glass slides grown for (a) 10, (b) 20, (c) 30, (d) 40 and (e) 60 min. (B) XRD patterns of hierarchical NC arrays on mica grown for (a) 10, (b) 30 and (c) 60 min. (C), XRD patterns of powder samples precipitated in solutions at (a) 40, (b) 60 and (c) 120 min. Adapted from ref 48.

began to form with the emergence of (311) and (222) peaks. After 60 min, the hierarchical mesophase crystals completely developed, each of which consisted of three to five uniformly merged subunit crystals. XRD (Fig. 7(A), curve (e)) revealed that the gold NC cubic mesophase was fully established by full appearance of (111), (220), (311) and (222) reflections. The enhanced intensity of the (111) and (222) XRD reflections during the crystal growth course (after 40 min) indicated an oriented growth with (111) planes parallel the substrate. This was consistent with the shapes of the mesophase crystal changing from triangular to hexagonal shape during the growth phase.

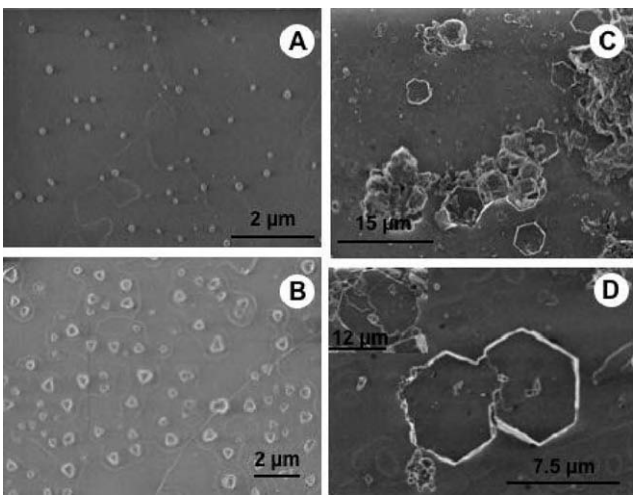

Fig. 8 SEM images of hierarchical NC arrays at different growth times: (A) 10 min; (B) 20 min; (C) and (D) 40 min. Adapted from ref 48.

Substrate surface properties strongly influence the nucleation and growth of inorganic materials.[68] In addition to amorphous glasses, we have conducted the crystal growth on mica substrates. In comparison with those grown on glass substrates, the crystals on the mica surface were fairly uniform in shape and size ($\sim$12 μm), but possessed circular rather than flower-like structure, and had only one single unit instead of several merged subunit crystals. Another apparent difference was that the crystal has an orientated feature on the mica surface with (111) planes parallel to the substrates. This could be due to the hexagonal crystalline surface that promotes preferential growth along (111) planes. Similar to the case of amorphous glass, the XRD patterns (Fig. 7(B), curves (b) and (c)), show enhanced reflections of the (111) and (222) planes suggesting the (111) planes of the NC cubic mesophase were parallel to the substrate. It was noteworthy that prior work in self-assembly of silica and surfactants indicated that only a one-dimensional hexagonal mesophase was formed.[69–71] It was proposed that surfactants formed hemirod micelles on the mica surface, leading to a one-dimensional surfactant/silica mesophase. In our systems, NC-micelles were preformed in a homogeneous aqueous solution. Self-assembly with organo-bridged silsesquioxane started with "hard sphere" NC-micelle building blocks instead of "soft" pure surfactant micelles or liquid crystals. Thus, the cubic mesophase was preferentially formed.

For growth times longer than 40 min a precipitate was observed. XRD patterns (Fig. 7(C)) on the precipitates showed irregular patterns, which suggested much less ordered/organized NC/silsesquioxane arrays. This unambiguously establishes that the mesophase crystals were grown from the solution rather than deposited *via* precipitation.

Thermal and mechanical stability is essential for NC arrays in practical nanodevice integrations. Heat treatment over time usually broadens the NC size distribution.[72] Our results showed that the organo-bridged silsesquioxane framework provided extensive protection from thermally induced particle agglomeration. TEM (Fig. 6(C) and (D)) has verified the monodispersity in the crystal arrays. UV-vis spectra further verified that the NC monodispersity was preserved inside the mesophase crystals after thermal annealing, showing no changes in the surface plasmon resonance band of the gold NC. This implied that the inorganic framework provided enhanced thermal stability. Additionally, in comparison with ordered NC superlattice films that exhibited cracking, these hierarchical NC mesophase crystals showed no cracking, unit cell distortion or shrinking even after heating to 100 °C for several hours, further confirming their mechanical stability.

4.2 Synthesis of ordered NC arrays in thin films

For device fabrication, thin films are more desirable than powders. The NC-micelles are water-soluble and allow to conduct sol–gel process to form ordered NC films through varied coating processes such as spin, cast and dip-coating, *etc.* To form thin films, we used acidic conditions designed to minimize the siloxane condensation rate (pH $\sim$ 2). By suppressing siloxane condensation and thereby gel formation, solvent evaporation accompanying coating induced self-assembly of NC-micelles into fcc NC thin film mesophases in a manner similar to the evaporation-induced self-assembly of cubic or hexagonal silica/surfactant thin film mesophases.[73,74] Silica condensation plays an important role in formation of ordered 3-D gold NC/silica arrays.[47] Oligosilica species in homogeneous coating solutions are essential to form ordered, transparent gold/silica thin films without cracking. Extensive silica condensation leads to less ordered gold/silica mesophase. By using organo-silsesquioxane, we were able to tune the framework chemistry and dielectrics. The final film consists of monodisperse gold NCs arranged within silica or organo-silsesquioxane host matrices in an fcc mesostructure with precisely controlled interparticle spacing.

The gold NC/silica films are transparent when less than 300 nm thick (Fig. 9(d)) and have an average refractive index of $\sim$1.7. The film thicknesses can be controlled from 100 nm to several micrometers depending on the spin rate or precursor concentration. The gold NCs inside the film remained monodisperse (Fig. 9(a)–(c)). This was further confirmed by TEM results and high resolution SEM images. Low-magnification SEM imaging (Fig. 10(A)) shows that the film had a uniform and continuous surface without macroscopic granularity or cracks. A high-resolution SEM image (Fig. 10(B)) confirmed that ordered gold NCs were distributed uniformly on the film surface.

The XRD pattern of the NC thin films were indexed as an fcc structure with unit cell $a \sim 10.5$ nm with primary peaks of (111), (220)/(311) and (222) reflections between 2θ 1 and 4°. After aging for 24 hours at room temperature, the film exhibited a lower degree of ordering with the disappearance of the (220)/(311) reflections and intensity decrease of (222)

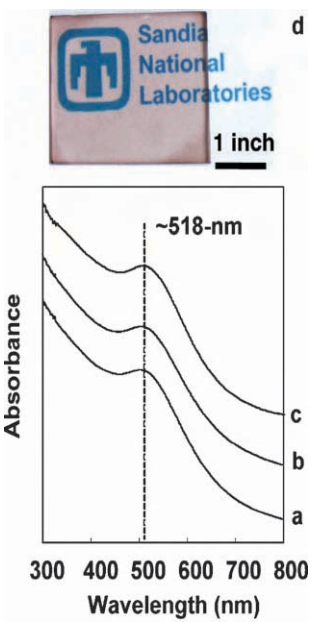

Fig. 9 UV-Vis spectra of (a) DT-stabilized gold NCs, (b) a gold NC/silica film prepared by using TEOS and (c) a gold/ethyl bridged silsesquioxane film prepared by using BTEE. (d) An optical micrograph of an as-prepared ordered gold/silica film on a glass substrate that covers the logo of Sandia National Laboratories. Adapted from ref. 49.

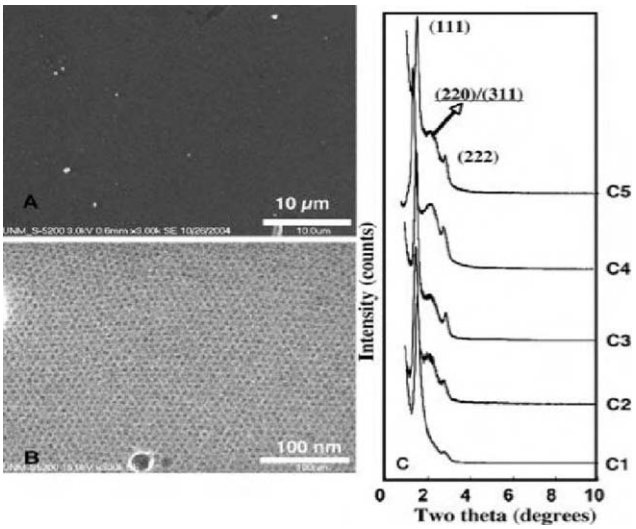

Fig. 10 (A) Low-resolution SEM image of an ordered gold NC/silica thin film. (B) High-resolution SEM image from the same specimen in (A). (C) XRD patterns of gold NC/silica films. Ordered gold/silica films prepared using a coating solution that was aged at ambient condition for (C1) 24 h and (C2) 5 h. (C3) Ordered gold/silica film prepared using a coating solution without aging. (C4) Ordered gold/silsesquioxane film prepared using a solution that was aged at ambient condition for 24 h. (C5) Ordered gold/silsesquioxane film prepared using a solution without aging. Adapted from ref. 49.

(Fig. 10(C1)). Periodically ordered regions were observed throughout the whole film thickness (Fig. 11(A)). The continuous and uniform air-film and film-substrate interfaces were consistent with SEM results showing no steps, kinks or cracking that appear in superlattice films prepared by evaporation of a NC solution.[20,43,75] The TEM images are consistent with an fcc structure (*Fm*3*m* space group) with a measured unit cell $a = \sim 10.8$ nm and a minimum average interparticle spacing of ~ 2.3 nm. It should be noted that the gold NC/silica thin film had a larger unit cell than that of previous superlattice films and solids[19,75] due to the silica layer between each of the individual gold NCs. As shown in plane-view image (Fig. 11(B)), regions of ordered gold NC arrays inside silica exhibited no preferred orientation with a seamless transition between ordered domains of gold NCs. Within the film, the gold NCs remained monodisperse.

We were able to tune the NC/silica mesophase from the cubic, gold NC/silica mesophase to a 2-D hexagonal silica/surfactant mesophase (Fig. 12, XRD patterns (C) and (D)) by reducing the concentration of the gold NCs, while maintaining a constant surfactant/silica molar ratio. Highly ordered NC mesophases also require very monosized NCs as was demonstrated by the broad, poorly-defined XRD pattern (Fig. 12(E)) obtained for a gold NC/silica powder sample prepared as in Fig. 12(B) but using gold NCs with rather broad size distribution synthesized according to Brust *et al.*[76]

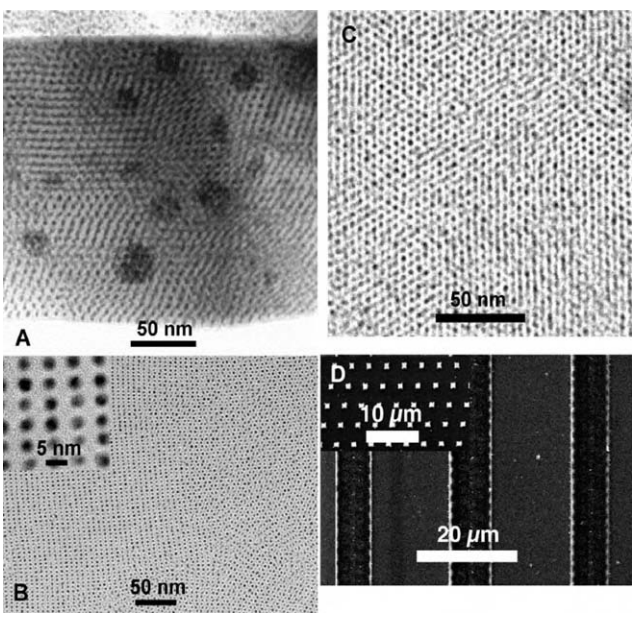

Fig. 11 (A) Cross-sectional TEM image of ordered gold NC/silica thin film. (B) Plane view TEM image of ordered gold NC/silica films through the complete film thickness showing the seamless transition within ordered domains. Inset, a high resolution TEM image. (C) Plane view TEM image of ordered gold NC/silsesquioxane films prepared by using BTEE. (D) Patterned gold NC/silica thin films using the micromolding method. Adapted from ref. 49.

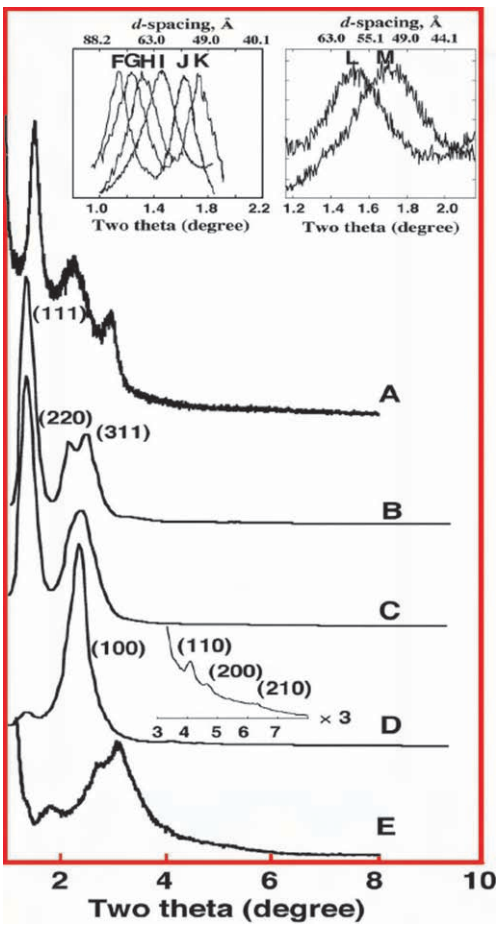

Fig. 12 XRD patterns of gold NC/silica mesophases. Insets (L) and (M) are magnifications of the (111) reflections plotted linearly for samples prepared as in (B) with two different secondary alkane chain lengths of the surfactant $(CH_3(CH_2)_n(NCH_3)_3{}^+Br^-$; $n_L = 15$, $n_M = 11$). Adapted from ref. 9.

As suggested by the bilayer structure of NC-micelle as shown in Fig. 1, the interparticle spacing or the lattice constant can be tuned by changing the primary NC particle size d_p, the primary layer thickness d_1, or the secondary layer thickness d_2. We have demonstrated the (111) *d*- spacing can be adjusted linearly from *ca.* 5.0 to 7.2 nm through variation of d_p from 1.0 to 3.3 nm. Insets L and M show that changing the secondary layer thickness d_2 by four carbon units ($CH_3(CH_2)_n$-$(NCH_3)_3{}^+Br^-$, n_L = 11 to n_K = 15) resulted in a 1.11 nm change in (111) *d*-spacing (1.38 Å per C–C bond) consistent with model predictions and structural studies.

Formation of ordered gold NC/silica thin films is analogous to that of self-assembly of surfactant and silica.[77] We proposed a cooperative self-assembly mechanism for the formation of ordered gold NC/silica mesophases[67] involving charge interaction and hydrogen bonding between hydrolyzed silica and surfactant head groups on the NC-micelle surface. Prior work on self-assembly and formation of surfactant and silica mesophases indicated that a series of mesophases were formed including lamellar, 1-d hexagonal, cubic, and 3-d hexagonal periodic symmetries depending on the surfactants, sol–gel process conditions, *etc*. In the case of NC-micelles and silica, only fcc mesostructures were preferentially formed regardless of basic and acidic catalytic conditions. This was due to the fact that the gold NC-micelles were pre-formed in a homogeneous solution and behaved rather like a "hard" sphere tending to form fcc close packing than "soft" pure surfactant micelles that are inclined to phase transformation. The method was flexible and allowed tuning of framework composition, and thus dielectrics, by using different sol–gel precursors. In addition to silica, we have demonstrated the synthesis of ordered gold NC arrays inside organo-silsesquioxane frameworks. Organo-bridged silsesquioxane is an ideal low *k* host, exhibiting chemical and mechanical robustness.[78,79] The ordered gold NC/silsesquioxane was prepared by using ~3 nm DM-stabilized gold NCs, CTAB and BTEE. The corresponding XRD patterns (Fig. 10(C4) and (C5)) and TEM image (Fig. 11) revealed that films exhibit ordered fcc mesostructure. In addition, the self-assembly, when using BTEE, was not strongly affected by solution aging unlike that when using TEOS. This was due to that the organo-bridged precursor had a relatively slower hydrolysis and condensation rate than TEOS.[80] Fig. 11(D) shows the patterned stripes and dots containing ordered gold NC/silica superlattices fabricated using micromolding techniques.[73]

Our method provides several advantageous features over previous methods. (1) The water-soluble NC-micelles allow the preparation of ordered NC arrays in aqueous phase, resulting in enhanced safety and better compatibility with current semiconductor fabrication processing. (2) Our method allows simple tuning of framework composition, thus dielectrics, between NCs. This is essential to achieve enhanced collective properties of such three-dimensional superlattice films.[31,81] Furthermore, the inorganic framework provides chemical and mechanical robustness,[82] and prevents films from cracking.

4.3 Integration of NC arrays for charge transport study

Ordered arrays of metallic NCs in silica are potential sources of implementation of several types of model systems offering a variety of opportunities to study the physics of transport. We have investigated the charge transport in ordered three-dimensional NC arrays, fabricated in planar metal-oxide-semiconductor (MOS) devices (see schematic in Fig. 13). The sample was initially biased at V_1 for 50 s, then rapidly switched (<1 μs) to V_2 and the time evolution of the capacitor charge monitored. We have observed an S-shaped profile with a ~7.5 s discharge time for the sample with gold NCs. Samples without gold exhibited normal *RC* discharge behavior (with a time constant ~100 μs). The total excess charge contained in this capacitor is approximately 2.8×10^{-11} C. Assuming the capacity of each NC to be one electron based on electrostatic energy considerations, this corresponds to 10^{18} cm^{-3} charged NCs. This was attributed to the charging of the gold in the oxide near the gate electrode when the gate was negatively biased. After reversing the gate voltage to V_2, the electrons on the gold NCs were swept out of the oxide into the gate sequentially from the gate side first. No change in substrate capacitance occurred until the gold NCs in the oxide were discharged as they effectively pin the Si-surface in accumulation. Using the fcc lattice constant, a uniform gold NC concentration was estimated in the oxide of $\sim 4 \times 10^{18}$ cm^{-3}. However, only those NCs located near the gate electrode could respond to the high frequency signal used to measure the capacitance, resulting in roughly *all* of the NCs in the first 25% of the oxide film being occupied by electrons. Given the spacing for these dots, Coulomb blockade effects were expected to control transport amongst the gold NCs. However, disorder and trapping within the silica matrix could prevent collective effects, so transport in this situation was probably also influenced by a combination of local kinetic and diffusive factors, particularly at room temperature where these experiments were performed. The charge storage and transport behavior was completely different from that of the corresponding MOS capacitor prepared without gold with silica identical to the host matrix of the NC array, and it was evident that charge was stored on the gold NCs and that the discharge characteristics were dominated by electron transport involving the NCs.

To further investigate the charge transport mechanism in our 3D arrays, we fabricated planar metal–insulator–metal (MIM) devices, incorporating an Au NC/silica array as the insulator layer (see schematic in Fig. 14), and measured their temperature dependent *I–V* characteristics.

At room temperature, the *I–V* curve was linear with a zero-biased resistance of 1 MΩ, corresponding to a film resistivity of about 3×10^6 ohm cm. Nonlinearity in the *I–V* behavior near zero bias was evident at 200 K and increased with decreasing temperature. At 100 K and below, conduction occurred through the gold NC/silica insulator only above a minimum threshold voltage, V_T, indicative of a collective Coulomb blockade[83] resulting from electrical isolation of the NCs. Comparison measurements on gold-free control samples showed no significant change in the *I–V* characteristics over this temperature range.

We observed temperature-dependent conductance of the Au/silica NC array (Fig. 14) and a strict Arrhenius behavior ($G_o \propto \exp[-E_c/k_bT]$) over the complete temperature range 77–300 K. This attests to the particle/array uniformity.

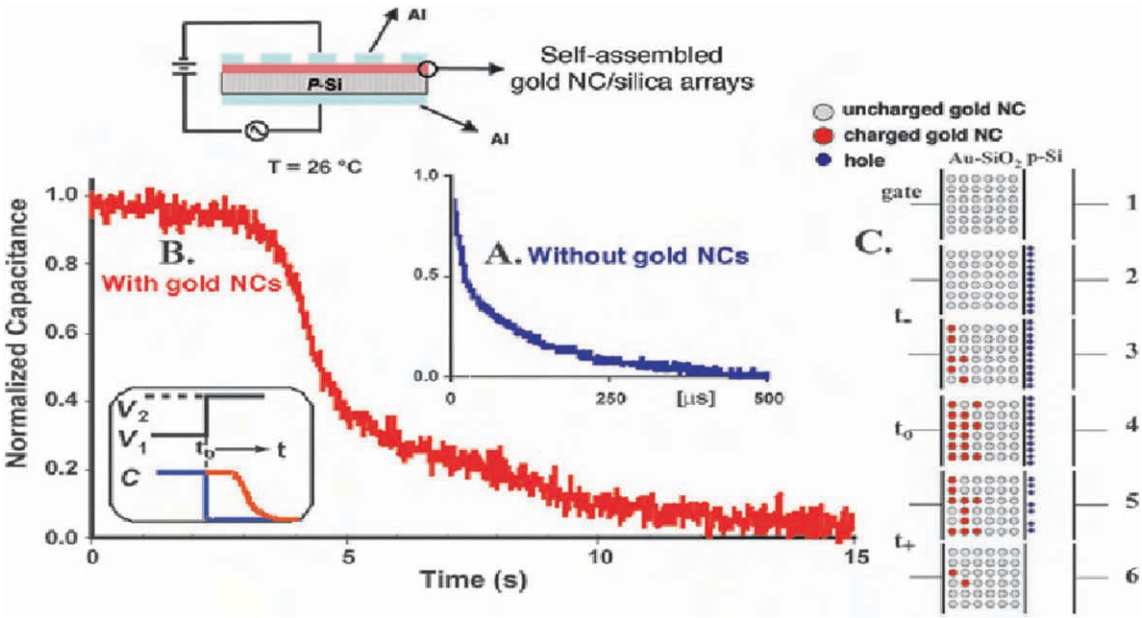

Fig. 13 Time dependence of normalized capacitance for MOS capacitors prepared using silica or ordered gold NC/silica as the 'oxide' dielectrics. The charge is measured when the capacitors are switched from V_1 to V_2. The discharge time for capacitors without gold NCs (A) is exponential with a characteristic time constant of ~100 μs. For gold NC-containing capacitors (B), the decay is no longer exponential and the discharge time (10–90%) is about 7.5 s. The time behavior of the discharge curve may be explained by following the biasing sequence shown in (C): (1) depicts an unbiased neutral p-type Si substrate; (2) shows that once a negative bias V_1 is placed on the gate, an accumulation of holes is quickly established at the Si-oxide interface. In (3) the capacitance of the device with gold NCs is higher than that of an equivalent gold NC-free device due to the excess stored charge in the gold levels. Experiments indicate that this process continues until all of the gold NCs in the first 25% of the oxide film near the gate are charged. Upon reduction of the gate bias to V_2 in (4), the accumulation layer begins to disappear. However, in (5) the accumulation layer is partially sustained in the presence of the charged gold NCs. Only as the electrons on the gold NCs move into the gate does the accumulation layer dissipate completely as shown in (6). The minimum capacitance for these structures occurs when the p-type semiconductor surface is biased into inversion. This value is the same for both gold NC and NC-free capacitors. Adapted from ref. 34.

Previous studies showed that 2D NC arrays and granular films in general often showed a $G_o \propto \exp[-(E_c/k_bT)^{1/2}]$ dependence caused by particle-size polydispersity.[84–86] We calculated the experimental value of the charging energy, E_c = 90 meV, determined from the slope in Fig. 14(A) (inset). This discrepancy between the experimental results and the prediction for an isolated NC reflected the reduction of the charging energy arising from the influence of the surrounding NCs. For 2-D NC arrays with sufficiently small NC spacings, both modeling and experiment showed the charging energy to vary reciprocally with the number of nearest neighbors.[84,87] Although 3-D models of the NC charging energy have not been formulated, it was anticipated that interparticle capacitance could easily account for the 33 meV reduction in E_c. observed here.

At low temperatures (T < 100 K) where we observed Coulomb blockade behavior, theory predicted that, for $V > V_T$, current scales as a power law, $I = I_o(V/V_T - 1)^{\zeta}$. The scaling exponent ζ reflected the dimensionality of the accessible current conducting pathways, and, for 1-D and 2-D systems, both modeling[84,87] and experiment[88] showed ζ to equal approximately the array dimensionality. Fig. 14(B) plots representative current–voltage scaling data for our 3D gold/silica NC arrays. Our results show at 77 K power law scaling with ζ = 2.7 (negative bias) and ζ = 3.0 (positive bias). To date, there are no theoretical predictions or simulations of the 3D scaling exponent, however the greater value of ζ observed here, compared to previous studies of 2D[88] and quasi-3D arrays,[84] is consistent with the greater number of conductive pathways expected for a fully 3D array.

5 Conclusions

The synthesis of NC-micelles represents a new synthetic methodology, enabling flexible NC surface chemistry and function. The method is easy, rapid (10 min), and avoids complicated multi-step surface functionalization procedures. The flexible surface chemistry and function provide a new interface for self-assembly and formation of ordered NC arrays with controlled morphology and framework that allows tuning of chemical and physical properties. The robustness of this approach should allow formation of a variety of other functional water-soluble nanomaterials such as C_{60}, carbon nanotubes and porphyrins that currently require complex procedures to achieve water solubility.

Acknowledgements

I warmly thank the collaborators and co-workers who contributed to these projects. Their names are mentioned in the associated publications quoted in the references. This work was supported by the U.S. DOE BES Program, Sandia National Laboratory's LDRD program, NINE program, NIMS program, CINT and NSF under Grant No. 0625897. TEM investigations were performed in the Department of Earth and

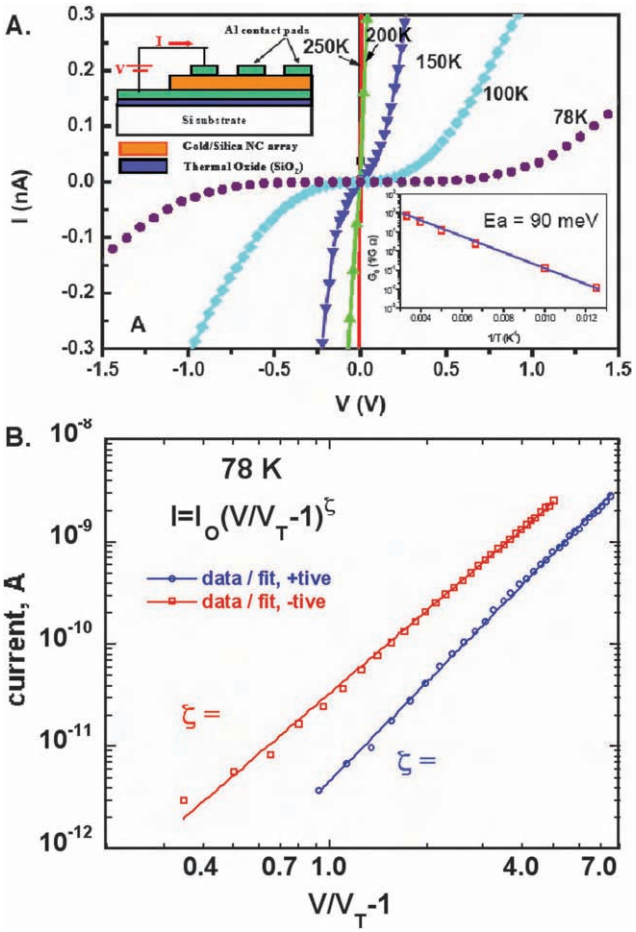

Fig. 14 (A) *I–V* curves measured from 300 to 78 K. The inset shows a plot of the zero-bias conductance (G_0) *vs.* $1/T$. The data exhibited Arrhenius behavior with activation energy (E_a) of ~90 meV. (B) At T = 78 K, the current displayed a power-law dependence for $V > V_T$ with scaling exponent ζ = 2.7 (negative bias) and ζ = 3.0 (positive bias). Adapted from ref. 9.

Planetary Sciences at the University of New Mexico. We acknowledge the use of the SEM facility supported by the NSF EPSCOR and NNIN grants. Sandia is a multiprogram laboratory operated by Sandia Corporation, a Lockheed Martin Company, for DOE under contract DE-AC04-94ALB5000.

References

1 T. S. Ahmadi, Z. L. Wang, T. C. Green, A. Henglein and M. A. El Sayed, *Science*, 1996, **272**, 1924.
2 A. P. Alivisatos, V. F. Puntes, K. M. Krishnan, M. Bruchez, M. Moronne, P. Gin and S. Weiss, *Science*, 1996, 933.
3 M. A. El-Sayed, *Acc. Chem. Res.*, 2001, **34**, 257.
4 S. H. Sun, *Adv. Mater.*, 2006, **18**, 393.
5 A. P. Alivisatos, K. P. Johnsson, X. G. Peng, T. E. Wilson, C. J. Loweth, M. P. Bruchez and P. G. Schultz, *Nature*, 1996, **382**, 609.
6 R. P. Andres, T. Bein, M. Dorogi, S. Feng, J. I. Henderson, C. P. Kubiak, W. Mahoney, R. G. Osifchin and R. Reifenberger, *Science*, 1996, **272**, 1323.
7 J. Chen, W. Wang, J. Klemic, M. A. Reed, B. W. Axelrod, D. M. Kaschak, A. M. Rawlett, D. W. Price, S. M. Dirk, J. M. Tour, D. S. Grubisha and D. W. Bennett, *Mol. Electron. II*, 2002, **960**, 69.
8 C. P. Collier, R. J. Saykally, J. J. Shiang, S. E. Henrichs and J. R. Heath, *Science*, 1997, **277**, 1978.
9 H. Y. Fan, K. Yang, D. M. Boye, T. Sigmon, K. J. Malloy, H. F. Xu, G. P. Lopez and C. J. Brinker, *Science*, 2004, **304**, 567.
10 V. I. Klimov, A. A. Mikhailovsky, S. Xu, A. Malko, J. A. Hollingsworth, C. A. Leatherdale, H. J. Eisler and M. G. Bawendi, *Science*, 2000, **290**, 314.
11 S. H. Sun, C. B. Murray, D. Weller, L. Folks and A. Moser, *Science*, 2000, **287**, 1989.
12 H. Zeng, J. Li, J. P. Liu, Z. L. Wang and S. H. Sun, *Nature*, 2002, **420**, 395.
13 M. P. Pileni, *J. Phys. Chem. B*, 2001, **105**, 3358.
14 C. B. Murray, C. R. Kagan and M. G. Bawendi, *Science*, 1995, **270**, 1335.
15 V. I. Klimov, A. A. Mikhailovsky, D. W. McBranch, C. A. Leatherdale and M. G. Bawendi, *Science*, 2000, **287**, 1011.
16 M. Kanehara, Y. Oumi, T. Sano and T. Teranishi, *J. Am. Chem. Soc.*, 2003, **125**, 8708.
17 A. M. Kalsin, M. Fialkowski, M. Paszewski, S. K. Smoukov, K. J. M. Bishop and B. A. Grzybowski, *Science*, 2006, **312**, 420.
18 G. A. DeVries, M. Brunnbauer, Y. Hu, A. M. Jackson, B. Long, B. T. Neltner, O. Uzun, B. H. Wunsch and F. Stellacci, *Science*, 2007, **315**, 358.
19 C. B. Murray, C. R. Kagan and M. G. Bawendi, *Annu. Rev. Mater. Sci.*, 2000, **30**, 545.
20 M. B. Sigman, A. E. Saunders and B. A. Korgel, *Langmuir*, 2004, **20**, 978.
21 D. V. Talapin, E.V. Shevchenko, A. Kornowski, N. Gaponik, M. Haase, A. L. Rogach and H. Weller, *Adv. Mater.*, 2001, **13**, 1868.
22 C. Murray, C. Kagan and M. Bawendi, *Annu. Rev. Mater. Sci.*, 2000, **30**, 545.
23 A. Badia, S. Singh, L. Demers, L. Cuccia, G. R. Brown and R. B. Lennox, *Chem.–Eur. J.*, 1996, **2**, 359.
24 Q. J. Guo, X. W. Teng, S. Rahman and H. Yang, *J. Am. Chem. Soc.*, 2003, **125**, 630.
25 E. V. Shevchenko, D. V. Talapin, S. O'Brien and C. B. Murray, *J. Am. Chem. Soc.*, 2005, **127**, 8741.
26 E. V. Shevchenko, D. V. Talapin, C. B. Murray and S. O'Brien, *J. Am. Chem. Soc.*, 2006, **128**, 3620.
27 F. X. Redl, K. S. Cho, C. B. Murray and S. O'Brien, *Nature*, 2003, **423**, 968.
28 A. Boker, Y. Lin, K. Chiapperini, R. Horowitz, M. Thompson, V. Carreon, T. Xu, C. Abetz, H. Skaff, A. D. Dinsmore, T. Emrick and T. P. Russell, *Nat. Mater.*, 2004, **3**, 302.
29 A. E. Saunders, P. S. Shah, M. B. Sigman, T. Hanrath, H. S. Hwang, K. T. Lim, K. P. Johnston and B. A. Korgel, *Nano Lett.*, 2004, **4**, 1943.
30 P. S. Shah, M. B. Sigman, C. A. Stowell, K. T. Lim, K. P. Johnston and B. A. Korgel, *Adv. Mater.*, 2003, **15**, 971.
31 J. Lee, V. C. Sundar, J. R. Heine, M. G. Bawendi and K. F. Jensen, *Adv. Mater.*, 2000, **12**, 1102.
32 M. A. Petruska, A. V. Malko, P. M. Voyles and V. I. Klimov, *Adv. Mater.*, 2003, **15**, 610.
33 H. Y. Fan, K. Yang, D. Boye, T. Sigmon, K. Malloy, H. Xu, G. P. Lopez and C. Brinker, *Science*, 2004, **304**, 567.
34 K. Yang, H. Y. Fan, K. J. Malloy, C. J. Brinker and T. Sigmon, *Thin Solid Films*, 2005, **491**, 38.
35 H. Y. Fan, Y. Q. Zhou and G. P. Lopez, *Adv. Mater.*, 1997, **9**, 728.
36 M. Epifani, C. Giannini, L. Tapfer and L. Vasanelli, *J. Am. Ceram. Soc.*, 2000, **83**, 2385.
37 D. K. Sarkar, F. Cloutier and M. A. El Khakani, *J. Appl. Phys.*, 2005, **97**, 084302.
38 A. Fukuoka, H. Araki, J. Kimura, Y. Sakamoto, T. Higuchi, N. Sugimoto, S. Inagaki and M. Ichikawa, *J. Mater. Chem.*, 2004, **14**, 752.
39 Y. Guari, C. Theiuleux, A. Mehdi, C. Reye, R. J. P. Corriu, S. Gomez-Gallardo, K. Philippot, B. Chaudret and R. Dutartre, *Chem. Commun.*, 2001, 1374.
40 Y. Guari, C. Thieuleux, A. Mehdi, C. Reye, R. J. P. Corriu, S. Gomez-Gallardo, K. Philippot and B. Chaudret, *Chem. Mater.*, 2003, **15**, 2017.
41 F. J. Brieler, M. Froba, L. M. Chen, P. J. Klar, W. Heimbrodt, H. A. K. von Nidda and A. Loidl, *Chem.–Eur. J.*, 2002, **8**, 185.
42 A. T. Cho, J. M. Shieh, J. Shieh, Y. F. Lai, B. T. Dai, F. M. Pan, H. C. Kuo, Y. C. Lin, K. J. Chao and P. H. Liu, *Electrochem. Solid State Lett.*, 2005, **8**, G143.
43 M. Pileni, *J. Phys. Chem. B*, 2001, **105**, 3358.

44 J. J. Urban, D. V. Talapin, E. V. Shevchenko, C. R. Kagan and C. B. Murray, *Nat. Mater.*, 2007, **6**, 115.
45 H. Y. Fan, E. Leve, J. Gabaldon, A. Wright, R. Haddad and C. Brinker, *Adv. Mater.*, 2005, **17**, 2587.
46 H. Y. Fan, Z. Chen, C. J. Brinker, J. Clawson and T. Alam, *J. Am. Chem. Soc.*, 2005, **127**, 13746.
47 H. Y. Fan, J. Gabaldon, C. J. Brinker and Y. B. Jiang, *Chem. Commun.*, 2006, 2323.
48 A. Wright, J. Gabaldon, D. B. Burckel, Y. B. Jiang, Z. R. Tian, J. Liu, C. J. Brinker and H. Y. Fan, *Chem. Mater.*, 2006, **18**, 3034.
49 H. Y. Fan, A. Wright, J. Gabaldon, A. Rodriguez, C. J. Brinker and Y. B. Jiang, *Adv. Funct. Mater.*, 2006, **16**, 891.
50 H. Y. Fan, E. W. Leve, C. Scullin, J. Gabaldon, D. Tallant, S. Bunge, T. Boyle, M. C. Wilson and C. J. Brinker, *Nano Lett.*, 2005, **5**, 645.
51 V. Patil, K. S. Mayya, S. D. Pradhan and M. Sastry, *J. Am. Chem. Soc.*, 1997, **119**, 9281.
52 L. F. Shen, P. E. Laibinis and T. A. Hatton, *Langmuir*, 1999, **15**, 447.
53 T. Pellegrino, L. Manna, S. Kudera, T. Liedl, D. Koktysh, A. L. Rogach, S. Keller, J. Radler, G. Natile and W. J. Parak, *Nano Lett.*, 2004, **4**, 703.
54 B. Dubertret, P. Skourides, D. J. Norris, V. Noireaux, A. H. Brivanlou and A. Libchaber, *Science*, 2002, **298**, 1759.
55 L. F. Shen, P. E. Laibinis and T. A. Hatton, *Langmuir*, 1999, **15**, 447.
56 L. E. Euliss, S. G. Grancharov, S. O'Brien, T. J. Deming, G. D. Stucky, C. B. Murray and G. A. Held, *Nano Lett.*, 2003, **3**, 1489.
57 H. Ai, C. Flask, B. Weinberg, X. Shuai, M. D. Pagel, D. Farrell, J. Duerk and J. M. Gao, *Adv. Mater.*, 2005, **17**, 1949.
58 B. S. Kim, J. M. Qiu, J. P. Wang and T. A. Taton, *Nano Lett.*, 2005, **5**, 1987.
59 S. Lecommandoux, O. Sandre, F. Checot, J. Rodriguez-Hernandez and R. Perzynski, *J. Magn. Magn. Mater.*, 2006, **300**, 71.
60 Y. F. Chen and Z. Rosenzweig, *Nano Lett.*, 2002, **2**, 1299.
61 Z. A. Peng and X. G. Peng, *J. Am. Chem. Soc.*, 2002, **124**, 3343.
62 D. S. Lidke, P. Nagy, R. Heintzmann, D. J. Arndt-Jovin, J. N. Post, H. E. Grecco, E. A. Jares-Erijman and T. M. Jovin, *Nat. Biotechnol.*, 2004, **22**, 198.
63 J. K. Jaiswal, H. Mattoussi, J. M. Mauro and S. M. Simon, *Nat. Biotechnol.*, 2003, **21**, 47.
64 K. Hanaki, A. Momo, T. Oku, A. Komoto, S. Maensono, Y. Yamaguchi and K. Yamaguchi, *Biochem. Biophys. Res. Commun.*, 2003, **302**, 496.
65 P. De Camilli, V. I. Slepnev, O. Shupliakov and L. Brodin, *Synaptic Vesicle Endocytosis*, ed. W. M. Cowan, T. C. Sudhof and C. F. Stevens, The Johns Hopkins Press, Baltimore and London, 2001.
66 T. Shitani and D. J. Klionsky, *Science*, 2004, **306**, 990.
67 Q. S. Huo, D. I. Margolese, U. Ciesla, P. Y. Feng, T. E. Gier, P. Sieger, R. Leon, P. M. Petroff, F. Schuth and G. D. Stucky, *Nature*, 1994, **368**, 317.
68 J. Aizenberg, A. J. Black and G. M. Whitesides, *Nature*, 1999, **398**, 495.
69 P. D. Yang, T. Deng, D. Y. Zhao, P. Y. Feng, D. Pine, B. F. Chmelka, G. M. Whitesides and G. D. Stucky, *Science*, 1998, **282**, 2244.
70 H. Yang, A. Kuperman, N. Coombs, S. Mamiche-Afara and G. A. Ozin, *Nature*, 1996, **379**, 703.
71 H. Yang, N. Coombs and G. A. Ozin, *Nature*, 1997, **386**, 692.
72 M. M. Maye, W. X. Zheng, F. L. Leibowitz, N. K. Ly and C. J. Zhong, *Langmuir*, 2000, **16**, 490.
73 H. Y. Fan, Y. F. Lu, A. Stump, S. T. Reed, T. Baer, R. Schunk, V. Perez-Luna, G. P. Lopez and C. J. Brinker, *Nature*, 2000, **405**, 56.
74 C. J. Brinker, Y. F. Lu, A. Sellinger and H. Y. Fan, *Adv. Mater.*, 1999, **11**, 579.
75 Z. L. Wang, *Adv. Mater.*, 1998, **10**, 13.
76 M. Brust, M. Walker, D. Bethell, D. J. Schiffrin and R. Whyman, *J. Chem. Soc., Chem. Commun.*, 1994, 801.
77 C. Kresge, M. Leonowicz, W. Roth, C. Vartuli and J. Beck, *Nature*, 1992, **359**, 710.
78 Y. F. Lu, H. Y. Fan, N. Doke, D. A. Loy, R. A. Assink, D. A. LaVan and C. J. Brinker, *J. Am. Chem. Soc.*, 2000, **122**, 5258.
79 H. Y. Fan, H. R. Bentley, K. R. Kathan, P. Clem, Y. F. Lu and C. J. Brinker, *J. Non-Cryst. Solids*, 2001, **285**, 79.
80 C. J. Brinker and G. W. Scherer, *Sol–Gel Science: the Physics and Chemistryof Sol–Gel Processing*, Academic Press Inc., New York, 1990.
81 V. C. Sundar, H. J. Eisler and M. G. Bawendi, *Adv. Mater.*, 2002, **14**, 739.
82 H. Fan, C. Hartshorn, T. Buchheit, D. Tallant, R. Assink, R. Simpson, D. J. Kissel, D. J. Lacks, S. Torquato and C. J. Brinker, *Nat. Mater.*, 2007, **6**, 418.
83 H. Grabert and M. H. Devoret, *Single Charge Tunneling*, Plenum, New York, 1992.
84 C. T. Black, C. B. Murray, R. L. Sandstrom and S. H. Sun, *Science*, 2000, **290**, 1131.
85 D. L. Peng, K. Sumiyama, S. Yamamuro, T. Hihara and T. J. Konno, *Appl. Phys. Lett.*, 1999, **74**, 76.
86 C. A. Neugebauer and M. B. Webb, *J. Appl. Phys.*, 1961, **33**, 74.
87 A. A. Middleton and N. S. Winggreen, *Phys. Rev. Lett.*, 1993, **71**, 3198.
88 A. J. Rimberg, T. R. Ho and J. Clarke, *Phys. Rev. Lett.*, 1995, **74**, 4714.

